Polaron Spin Current Transport in Organic Semiconductors

Shun Watanabe*,[1] Kazuya Ando* †,[2,3,4] Keehoon Kang,[1] Sebastian Mooser,[1] Yana Vaynzof,[1] Hidekazu Kurebayashi,[1,4] Eiji Saitoh,[3,5,6,7] and Henning Sirringhaus‡[1]

[1]*Cavendish Laboratory, University of Cambridge, J. J. Thomson Avenue, Cambridge CB3 0HE, United Kingdom*

[2]*Department of Applied Physics and Physico-Informatics, Keio University, Yokohama 223-8522, Japan*

[3]*Institute for Materials Research, Tohoku University, Sendai 980-8577, Japan*

[4]*PRESTO, Japan Science and Technology Agency, Sanbancho, Tokyo 102-0075, Japan*

[5]*WPI Advanced Institute for Materials Research, Tohoku University, Sendai 980-8577, Japan*

[6]*CREST, Japan Science and Technology Agency, Sanbancho, Tokyo 102-0075, Japan*

[7]*The Advanced Science Research Center, Japan Atomic Energy Agency, Tokai 319-1195, Japan*

* These authors contributed equally to this work

† Correspondence and requests for materials should be addressed to ando@appi.keio.ac.jp

‡ Correspondence and requests for materials should be addressed to hs220@cam.ac.uk

In spintronics pure spin currents play a key role in transmitting, processing, and storing information. A pure spin current is a flow of electron spin angular momentum without simultaneous flow of charge current. It can be carried by conduction electrons or magnons and has been studied in many inorganic metals, semiconductors and insulators, but not yet in organic semiconductors. Charge carriers in π-conjugated organic materials are localised, spin-1/2 polarons which move by hopping but the mechanisms of their spin transport and relaxation are not well understood. Here we use ferromagnetic resonance spin pumping in a ferromagnet/conjugated polymer/nonmagnetic spin-sink trilayer to demonstrate the ability of polarons to carry pure spin currents over hundred nanometers with long spin relaxation time up to a millisecond and to exhibit Hanle precession. By systematically comparing charge and spin transport on the same trilayer we show that spin-orbit coupling mediates spin relaxation at room temperature.

Organic semiconductors (OSCs) are being investigated as an emerging class of materials for electronics and spintronics, not only because of their ease of low-temperature solution processing, but also because of their unique functional properties, such as a long spin lifetime that reflects their light-atom, mainly carbon-based composition. To date, the focus in organic spintronics has mainly been on studies of spin valves with a thin organic semiconductor layer sandwiched between two ferromagnetic electrodes.[1–3] In organic spin valves a spin polarised current is electrically injected from an adjacent ferromagnetic electrode and transported through the OSC. However, the concept of pure spin current, which carries purely spin angular momentum but, in contrast to a spin polarised current, no charge current,[4–9] had not been observed in organic materials until very recently. Apart from offering technological benefits, such as reduced heat dissipation compared to charge current based information processing, pure spin currents also allow observation of new physics, such as the conversion of a spin current into a transverse charge current through the spin-orbit coupling mediated inverse spin Hall effect (ISHE).[10–12] Recently, we realised spin pumping at the interface between a ferromagnetic insulator and a conducting polymer and we reported the first observation of pure spin currents and the ISHE in a highly doped, conducting polymer.[13] In the present work we extend our studies of spin pumping and pure spin currents to

undoped, semiconducting conjugated polymers.

Charge carriers in conjugated polymers are polarons formed as a result of strong electron-phonon coupling and move by hopping with a mobility that decreases with decreasing temperature.[14] While a detailed molecular understanding of charge transport has been achieved in a broad range of materials systems, the mechanisms for transport and relaxation of a spin polarisation generated among these spin 1/2 carrying polarons are much less well understood.[2,15] Generally the spin-orbit coupling (SOC) mediated Elliott-Yafet[16] and the hyperfine[17] mechanisms are most relevant in undoped, conjugated polymers, but a consensus about the dominant mechanism, particularly near room temperature, has so far not emerged. This is at least partly due to practical limitations of spin-valve measurements, which have been the only tool to investigate spin transport in OSCs. They suffer from the resistance mismatch problem that makes it difficult to efficiently inject spins from high conductivity metals into relatively low conductivity OSCs and have often been limited to low temperatures.[1–3] Our new trilayer architecture relies on spin pumping from a ferromagnetic material for spin injection into the OSC and on the ISHE in a nonmagnetic metal with strong SOC for detection of spins transmitted through the OSC. It allows us to measure in the same device both spin and charge carrier transport through the OSC.

Our trilayer device structure (Fig. 1a) uses a ferromagnetic (FM) metal of $Ni_{80}Fe_{20}$ in contact with the OSC to excite ferromagnetic resonance (FMR) and induce spin pumping[8–10,18] into the OSC. The FMR spin pumping generates a spin current from the precession of the magnetization, $\mathbf{M}$, at the FM metal/OSC interface, which is pumped out of the FM into the OSC mediated by the interlayer exchange coupling.[19] The injected, pure spin current is then transported through the OSC film until it reaches a thin Pt layer on the other side of the OSC film, where it is converted into an electric field $\mathbf{E}_{\mathrm{ISHE}}$ by the ISHE of Pt. $\mathbf{E}_{\mathrm{ISHE}}$ is perpendicular to both the directions of the spin polarisation and the spin current, $\mathbf{E}_{\mathrm{ISHE}} \propto \mathbf{j}_{\mathrm{s}} \times \boldsymbol{\sigma}$ (Fig. 1a),[10,20] where $\mathbf{j}_{\mathrm{s}}$ and $\boldsymbol{\sigma}$ denote the flow direction of the spin current and the spin-polarisation vector of the spin current. We use Pt because of its strong SOC which generates a large ISHE voltage signal, V_{ISHE}, between two contacts made to opposite ends of the Pt film. Injection and detection of a pure spin current is well established in metals[20] and inorganic semiconductors,[18,21] and more recently, in highly-doped conducting polymers.[13] In this work we study the transport of pure spin currents through the semiconducting conjugated polymer, poly(2,5-bis(3-alkylthiophen-2-yl)thieno[3,2-*b*]thiophene) (PBTTT, Fig. 1b).

PBTTT is a widely studied conjugated polymer with a high, in-plane field-effect mobility around 1 $cm^2V^{-1}s^{-1}$.[22] Figure 1c shows a cross-sectional transmission electron microscope image of a $Ni_{80}Fe_{20}$ (10 nm)/PBTTT (20 nm)/Pt (7 nm) trilayer, in which the PBTTT film was spin coated onto the Pt layer (supplementary information (SI) section A). The interfaces between PBTTT and the electrodes are smooth and abrupt (see also the atomic force microscopy images in SI section B); intermixing at the hybrid organic-inorganic interfaces is negligible. The PBTTT films are not intentionally doped but they contain a residual concentration of mobile polarons on the order of $10^{15} - 10^{16}$ cm^{-3} due to unintentional doping and/or thermal injection from the electrodes (see SI sections C and D). The resistivity of the PBTTT film was determined to be 1.8 GΩ cm. As a result of this high resistivity the PBTTT films provide electrical isolation between the $Ni_{80}Fe_{20}$ and Pt layers. The resistance of the trilayer between the $Ni_{80}Fe_{20}$ and Pt is determined to be over 70 kΩ from current-voltage measurements. From this we also exclude the presence of electrical shorts between the two metals. This electrical isolation is important, as will be discussed below. It minimizes the transmission of spurious voltage signals generated in the $Ni_{80}Fe_{20}$ into the Pt detector.

In such trilayers we studied the transport of pure spin currents through the PBTTT layer. Figures 2a and 2c show the microwave absorption I and the DC electromotive force V signal at 100 mW microwave excitation on a $Ni_{80}Fe_{20}$ (10 nm)/PBTTT (40 nm)/Pt (7 nm) sample. A voltage signal appears at the FMR field (H_{FMR}). Its sign is reversed when reversing the in-plane magnetic field direction from $\mathbf{H}$ to $-\mathbf{H}$ (Fig. 2b). This is consistent with the voltage being generated by the ISHE in the Pt layer.[20]

Importantly, the observed voltage was found to scale with the magnitude of the spin Hall angle of the nonmagnetic metal (NM) layer. The voltage signal for a $Ni_{80}Fe_{20}$ (10 nm)/PBTTT (40 nm)/Au (40 nm), in which Pt is replaced by Au, significantly decreases (Fig. 2d), and no voltage signals were detected in a $Ni_{80}Fe_{20}$ (10 nm)/PBTTT (40 nm)/Cu (300 nm) trilayer (Fig. 2e). The relative magnitude of the voltage detected for the different metals is quantitatively consistent with the theory of the ISHE in the NM metal (see Method section) and the measured voltage ratio for Pt and Au is much larger than the simple resistance ratio, $\frac{1}{d^{\mathrm{Pt}}\sigma^{\mathrm{Pt}}}/\frac{1}{d^{\mathrm{Au}}\sigma^{\mathrm{Au}}} \sim R^{\mathrm{Pt}}/R^{\mathrm{Au}} = 6.98$, where d^{NM}, σ^{NM} and R^{NM} are the film thickness, electrical conductivity and resistance of the NM layer. This shows that the difference in voltage signals for the different metals is not a mere effect of voltage shunting

(see Method section and SI section E). No voltage can be observed for Cu since the spin Hall angle of Cu is much smaller than those for Pt and Au.[23] Figure 2f shows the V spectrum for a $Ni_{80}Fe_{20}$ (10 nm)/CYTOP (60 nm)/Pt (7 nm) trilayer. CYTOP is an amorphous fluoropolymer polymer. Unlike semiconducting PBTTT with its residual mobile polaron concentration CYTOP is an ideal insulator (resistivity $\sim 10^{17}$ Ω cm) without π-conjugation (see chemical structure in the inset of Fig. 2f). Therefore, spins can no longer be transmitted due to the absence of carriers. This demonstrates that the FMR spin current can only be transmitted through π-conjugated, semiconducting organic materials in which a sufficient concentration of spin-carrying polarons is present. We also considered and excluded several potential experimental artefacts (see Method section and SI section D,G). By considering the equivalent circuit model in Fig. 2g, we found that since the $Ni_{80}Fe_{20}$ and bottom NM layers are electrically isolated by the inserted PBTTT layer, any electromotive force in the $Ni_{80}Fe_{20}$ is shunted and should not contaminate the output voltage in the Pt layer (SI section F).

Since the voltage generated in the Pt layer should be linearly proportional to the magnitude of the pure spin current that arrives at the Pt layer after being transmitted through the PBTTT film, voltage measurements as a function of thickness, d_s, of the PBTTT layer provide a means to probe the spin current transport through the conjugated polymer. Remarkably, we can detect a clean ISHE signal up to relatively large PBTTT thicknesses of a few 100 nm's (Figure 2h). V_{ISHE} decreases with increasing PBTTT thickness and this decrease is well-approximated by an exponential decay, $V_{ISHE}(d_s) \propto e^{-d_s/\lambda_s}$, with a decay constant $\lambda_s = 153 \pm 32$ nm. The exponential decay provides further proof that the measured voltage is generated by the ISHE in the NM rather than by a spurious voltage signal generated in the $Ni_{80}Fe_{20}$ layer. The transmission of such signals through the PBTTT layer would be expected to depend on the PBTTT resistance, in which case V_{ISHE} would be expected to scale not exponentially but as $1/d_s$ (see SI section F). The observation of an exponential decay also suggests that the spin current is transported through the PBTTT film by diffusion and we interpret the decay constant as the spin diffusion length of the PBTTT layer. In the following we will adopt a theoretical framework based on the spin diffusion equation that has been widely used for interpreting spin pumping measurements on inorganic semiconductors and metals[18,20,21] but can also be justified in organic semiconductors.[24]

The voltage spectra were also measured as a function of the out-of-plane angle θ between

the substrate plane and the static magnetic field as defined in Fig. 3a. The electric voltage $\bar{V}_{\mathrm{ISHE}}$, defined as the V_{ISHE} normalized by the microwave absorption at each θ, is shown as a function of θ in Fig. 3b. The $\bar{V}_{\mathrm{ISHE}}$ signal disappears at $\theta = 90°$ and 270°, and the sign of the voltage is reversed at $\theta = 180°$, which is consistent with the symmetry of the ISHE.[20] Such angular measurements provide information about the Hanle precession of the spin polarisation around the magnetic field direction present in the PBTTT layer. This is because the injected spin polarisation $\boldsymbol{\sigma}$ at the interface between $Ni_{80}Fe_{20}$ and PBTTT is directed along the magnetization precession axis ϕ, which is different from θ because of the magnetic anisotropy of the $Ni_{80}Fe_{20}$ layer. The angle ϕ is obtained from the θ dependence of the resonance field H_{FMR} (Fig. 3c) using the Landau-Lifshitz-Gilbert equation.[20] The magnetization-precession axis is mostly confined along the in-plane direction except when θ is nearly 90° and 270° (Figure 3d). In other words, $\boldsymbol{\sigma}$ at the interface is almost parallel to the film plane except for nearly 90° and 270°. When $\mathbf{H}$ is applied oblique to the film plane, the spins injected into the OSC precess around $\mathbf{H}$ according to the Hanle effect.

In materials with long spin lifetime, the spin current that arrives at the PBTTT/Pt interface is expected to be $j^z_{\mathrm{s},x}(d_{\mathrm{s}}) \sim j_{\mathrm{s}} \cos\theta \cos(\theta - \phi) e^{-d_{\mathrm{s}}/\lambda_{\mathrm{s}}}$. Thus, $V_{\mathrm{ISHE}} \propto \cos\theta \cos(\theta - \phi)$ because the spin relaxation time in Pt is very fast (see Method section). The experimentally measured $\bar{V}_{\mathrm{ISHE}}$ is well reproduced with this model but not with the simple $\cos\phi$ relationship that would be expected if spins in PBTTT had a short spin lifetime and were effectively not precessing. These measurements therefore provide evidence for Hanle precession in PBTTT. The Hanle spin precession of polarons observed here has been a missing part in the organic spintronics field for many years.[15] The model does not allow a precise determination of the spin relaxation time, τ_{s}. We can only state that τ_{s} must be larger than approximately 1 ns (red curve in Fig. 3b and Method section).

We summarize our key experimental observations: (i) The magnitude of the ISHE voltage scales with the spin Hall angle of the NM layer. (ii) The ISHE voltage decays exponentially as the PBTTT thickness increases. (iii) The angular dependence of the ISHE voltage is consistent with the injected spins undergoing Hanle precession around the external field direction in the organic semiconductor. We emphasize again that by choosing a non-intentionally doped organic semiconductor layer with a high resistance we decouple potential spurious voltage signals generated in the permalloy from the Pt spin detector layer and eliminate experimental artefacts. Our observations provide convincing evidence that polarons in the

polymer semiconductor are able to transport a pure spin current through relatively thick organic semiconductor layers with thicknesses on the order of a few 100 nms.

The present trilayer architecture provides a powerful architecture for studying the currently not well understood mechanisms for spin diffusion in OSCs.[3] It does not suffer from the resistance mismatch problem and allows us to relate charge carrier mobility and spin diffusion length on the same device structure over a wide temperature range. Figure 4a shows the temperature, T, dependence of $\bar{V}_{\mathrm{ISHE}}$ measured for $Ni_{80}Fe_{20}$ (10 nm)/PBTTT (d_{s})/Pt (7 nm) trilayer devices with different PBTTT thicknesses d_{s}. For all devices the measured voltages are almost independent of T. At each temperature, $\bar{V}_{\mathrm{ISHE}}$ decays exponentially as d_{s} increases (Fig. 4b). The extracted values for λ_{s} (top panel of Fig. 4d) are approximately temperature-independent. For the set of samples used in the temperature dependent experiments we extracted a slightly larger value of $\lambda_{\mathrm{s}} = 200 \pm 30$ nm than found for the first set of samples used for room temperature measurements (Fig. 2h). To extract the corresponding spin relaxation time we measured the current-voltage (J-V) characteristics for the $Ni_{80}Fe_{20}$ (10 nm)/PBTTT (120 nm)/Pt (7 nm) trilayer diodes (Fig. 4c) using either the $Ni_{80}Fe_{20}$ (10 nm) or the Pt layer as good hole injecting contacts. This allows extraction of charge carrier mobilities from the standard quadratic current-voltage dependence in the space-charge-limited-current (SCLC) conduction regime.[25] From fits to Child's law, $J \propto \mu V^2$, the mobility μ was determined (middle Fig. 4d). μ exhibits a pronounced decrease with decreasing temperature that follows an approximate thermal activation behaviour and indicates that polaron transport in PBTTT occurs by hopping. Given this strong temperature dependence of the mobility the temperature independence of λ_{s} is a remarkable result.

In a hopping transport regime, the spin diffusion length and spin relaxation time can be related via the diffusion coefficient D, $\lambda_{\mathrm{s}} = \sqrt{D\tau_{\mathrm{s}}}$. The validity of the Einstein relationship in this transport regime, $D = k_{\mathrm{B}}T\mu/e$, has been established by recent experimental[26] and theoretical studies.[24] This allows us to extract values for τ_{s} from the measured values of μ and λ_{s}. In contrast to λ_{s}, τ_{s} increases strongly with decreasing temperature and reaches values up to 20 milliseconds at 200 K (bottom panel of Fig. 4d).

From the observed temperature dependence of τ_{s} and μ important conclusions can be drawn about the dominant mechanism for spin relaxation in PBTTT. We can neglect hyperfine coupling in our spin-pumping experiments (SI section G). Considering SOC according to the Elliott-Yafet (EY) mechanism[16] spins can undergo spin-flip scattering during an

ordinary momentum scattering event since SOC causes the spin wavefuctions to have an admixture of the opposite spin states.[4,27] In trap-free inorganic materials this leads to the spin relaxation rate τ_s^{-1} being proportional to the momentum scattering rate τ_p^{-1}, where τ_p is the momentum relaxation time. As a result τ_s typically becomes longer at low temperatures as momentum scattering becomes less frequent and the mobility $\mu = e\tau_p/m$ increases (m is the charge carriers' effective mass). In disordered PBTTT this argument cannot be used directly to explain the long spin relaxation times at low temperatures as the mobility at low temperatures becomes limited by charge carrier trapping and detrapping. However, in a trap limited EY system one still expects the spin relaxation time to increase with decreasing temperature since the spins are protected from spin-flip scattering while they reside in the trap states. Spins can only be flipped while carriers are moving in between two trapping events. In this regime one expects $\tau_s \propto \tau_{tp} \propto \mu^{-1}$, where τ_{tp} is the characteristic trapping time, which increases with decreasing temperature. This model based on SOC provides a consistent explanation of the observed temperature dependence of τ_s. In contrast, such a behaviour is difficult to explain with a spin relaxation mechanism based on the hyperfine interaction since one would expect a decrease of τ_s in the trap dominated transport regime at low temperatures (see SI section G), which is clearly inconsistent with the experimental data. We therefore conclude that a SOC-based mechanism based on the EY interaction provides a consistent explanation of our spin pumping experiments on PBTTT in the temperature range between 200 to 300 K.

These conclusions are fully consistent with recent temperature-dependent electron spin resonance measurements on gate-induced polarons in PBTTT films.[28] They are also in a good agreement with a recent theoretical study,[24] in which spin-flip and spin-conserving hopping at spin scattering centres in OSCs have been theoretically addressed. The theory postulates that, in a hopping regime, the spin diffusion length is directly proportional to the characteristic hopping distance, $\overline{R}$, renormalised by the strength of SOC as measured by a dimensionless parameter γ, $\lambda_s \propto \frac{\overline{R}}{\gamma}$. In this model a large and temperature-independent value of λ_s on the order of 100's nm as observed here is expected for systems with weak SOC (γ on the order of $10^{-3} - 10^{-4}$ from experimentally observed g-value shifts)[28] and a temperature-independent hopping length of several nm's.

In our analysis we have assumed that spin diffusion is the dominant mechanism for spin transport through the organic layer and that a formalism based on the spin diffusion equa-

tion, which is normally applied to metals with constant density of states, can be applied to organic semiconductors. The use of the spin diffusion equation for organic semiconductors has been justified in a previous theoretical study[24] and it provides a consistent explanation of our key experimental observations, such as the exponential dependence of the voltage on polymer thickness and the temperature independence of λ_s. However, there is one open question that warrants further discussion. To generate the sizeable voltage signal in the Pt requires the spin current transmitted through the polymer to be relatively large. To explain this we need to assume either a spin conductivity in the PBTTT that is several orders of magnitude higher than what is expected from the measured electrical conductivity of the polymer and/or an exceptionally large ($> 1\mu$eV) splitting of the chemical potentials for spin-up and spin-down electrons at the $Ni_{80}Fe_{20}$/PBTTT interface. The latter might arise as a result of the spin battery effect[29] and the long spin relaxation time of PBTTT. The former could be caused, for example, by exchange contributions to spin diffusion.[30] Exchange-mediated spin diffusion relies on quantum mechanical exchange coupling of spins that come close to each other on adjacent sites without requiring physical hopping of the associated charges and has been predicted to become dominant over polaron hopping mediated spin diffusion and lead to order of magnitude enhancements of the spin diffusion coefficients in a polaron concentration regime of $10^{16} - 10^{17}$ cm^{-3}, depending on the value of the localization length of the polaron wavefunction. This is the concentration regime present in our films due to unintentional doping / thermal injection from the contacts. If exchange enhanced spin diffusion was indeed relevant, the only level of analysis in this work that might have to reevaluated are likely to be the quantitative values of the spin relaxation time, which were extracted by assuming the simple Einstein relationship. Clearly, future work is needed to clarify the origin of the large spin current, and we hope that our work will encourage theoretical groups to develop a microscopic framework in which spin pumping measurements and spin transport in relatively resistive organic semiconductors with low carrier concentration can be interpreted quantitatively.

The temperature-independent spin diffusion length implies that improvements in polaron mobility will not necessarily result directly in increases of spin diffusion length. A new molecular design approach for tuning molecular packing and the strength of SOC is needed to further lengthen spin diffusion lengths and spin relaxation times. An intrinsic "low-mobility" may not be an inherent disadvantage. Our trilayer FM/OSC/Pt architecture is

widely applicable to many OSCs and temperature regimes and opens up new opportunities for fully understanding the spin transport and spin relaxation mechanisms in OSCs.

Method

ISHE voltages in the trilayer structure To interpret the magnitude of the voltage with the different metals quantitatively we assume that a fraction j_s of the spin current density injected into the PBTTT is transmitted through the PBTTT layer and arrives at the interface with the bottom NM metal layer, where it is transmitted into the NM metal layer and is converted into a voltage by the ISHE in the NM metal layer. j_s is independent of the NM layer. The theoretically expected magnitude of V_{ISHE} can be obtained from the equivalent circuit model of the ISHE induced by a spin current injected into the NM metal with spin Hall angle θ_{SHE}^{NM}, spin diffusion length λ^{NM}, film thickness d^{NM} and electrical conductivity σ^{NM} [31] (more details are shown in SI section E)

$$V_{ISHE} = \frac{2ew_F}{\hbar} j_s \frac{\theta_{SHE}^{NM} \lambda^{NM} \tanh(\frac{d^{NM}}{2\lambda^{NM}})}{d^{NM}\sigma^{NM}}, \quad (1)$$

w_F is the width of the $Ni_{80}Fe_{20}$ layer. Since we chose the thicknesses of the spin sink layers to scale with the literature values of the spin diffusion lengths in Pt, Au, and Cu (i.e., the factors d^{NM}/λ^{NM} and $\tanh(d^{NM}/2\lambda^{NM})$ in equation (1) are adjusted to be similar among the NM layers), the measured voltage ratio of devices with different NM layers should scale simply with the spin Hall angle and electrical conductivity of the NM layer as $V_{ISHE}^{Pt}/V_{ISHE}^{Au} = \frac{\theta_{SHE}^{Pt}}{\sigma^{Pt}}/\frac{\theta_{SHE}^{Au}}{\sigma^{Au}}$. Using experimental values for $V_{ISHE}^{Pt} = 0.956\ \mu V$, $V_{ISHE}^{Au} = 0.026\ \mu V$, $\sigma^{Pt} = 6.17 \times 10^6\ Sm^{-1}$, $\sigma^{Au} = 1.23 \times 10^7\ Sm^{-1}$, and literature values for $\theta_{SHE}^{Pt} = 0.04$[20] and $\theta_{SHE}^{Pt} = 0.0035$,[32] we find that the ratios of $V_{ISHE}^{Pt}/V_{ISHE}^{Au} = 36.8$ and $\frac{\theta_{SHE}^{Pt}}{\sigma^{Pt}}/\frac{\theta_{SHE}^{Au}}{\sigma^{Au}} = 33.5$ are consistent with each other. This strongly suggests that the spin Hall angle of the NM layer is responsible for the measured voltages as predicted by the trilayer spin pumping model (equation (1)) and that contributions from the weak ISHE in the OSC[13] can be neglected in this measurement configuration.

Voltage artefacts generated in the $Ni_{80}Fe_{20}$ A potential artefact in the present measurements could arise from spurious electromotive forces generated under FMR conditions in the $Ni_{80}Fe_{20}$, such as the anomalous Hall effect, the ISHE in the $Ni_{80}Fe_{20}$ due to backflow of spins from the interface[33] or any magneto-galvanic, microwave heating or magnetoresistance effects. To exclude this a series of further control experiments was performed. In order to shunt efficiently any spurious signals that might be generated in the $Ni_{80}Fe_{20}$ we deposited a high conductivity shorting bar of Al onto the surface of the $Ni_{80}Fe_{20}$, which reduced the resistance of the top metal layer from 180 Ω for $Ni_{80}Fe_{20}$ to 2 Ω for $Al/Ni_{80}Fe_{20}$. The detected

ISHE signal in the Pt was unaffected demonstrating convincingly that the high resistance of the OSC isolates the Pt detector from any voltage artefacts generated in the $Ni_{80}Fe_{20}$. H-dependent effects like Hall and Nernst effects, and M-dependent effects like anomalous Hall and anomalous Nernst effects can be excluded by considering the symmetry of the ISHE and frequency dependent measurements (SI section H). We have also confirmed that there is no measurable OMAR effect in this system (SI section D).

Analysis of the Hanle precession By assuming that there is no spin back-reflection at the interface between the OSC and the spin-sink Pt layer the z-component of the spin polarisation at a depth x in the PBTTT film can be approximated as[21]:

$$j^z_{s,x}(x) \propto \cos\theta\cos(\theta-\phi)e^{-x/\lambda_s} + \sin\theta\sin(\theta-\phi)\mathrm{Re}\left[e^{-x/\lambda_\omega}\right], \quad (2)$$

where $\lambda_\omega = \lambda_s/\sqrt{1+i\omega_L\tau_s}$, and $\omega_L = \gamma_C H_{FMR}$. γ_C and τ_s are the gyromagnetic ratio and spin relaxation time of PBTTT, respectively. We computed the angular variation of the $\bar{V}_{ISHE}$ with various spin relaxation times τ_s, where $\bar{V}_{ISHE}$ is proportional to the spin current density that arrives at the Pt layer ($x = d_s$). We assumed that the spin diffusion length λ_s is independent of τ_s, which is confirmed to be valid by our experimental results shown in Fig. 4d. In systems with short spin relaxation time $\omega_L\tau_s \ll 1$ this leads to a simple $\cos\phi$ angular dependence, which is clearly inconsistent with the experimental data (see dotted curves with $\tau_s \leq 0.1$ ns in Fig. 3b). As $\bar{V}_{ISHE}$ follows the predicted angular dependence and spins can clearly respond at the FMR frequency, the spin relaxation time is at least much longer than the timescale defined by the Larmor frequency ($\omega_L = \gamma_C H_{FMR} \geq 2.2\times10^{10}$ s^{-1}). In principle, it should in the future be possible to obtain a more accurate estimate of τ_s from Hanle measurements but this will require us to adjust the resonance condition by tuning f and H_{FMR} in order to resolve longer spin relaxation times. We show in Fig. 4 that τ_s is in fact significantly longer than our current Hanle-based lower limit estimate, i.e. on the order of μs.

---

[1] Xiong, Z. H., Wu, D., Vardeny, Z. V. & Shi, J. Giant magnetoresistance in organic spin-valves. *Nature* **427**, 821–824 (2004).

[2] Szulczewski, G., Sanvito, S. & Coey, M. A spin of their own. *Nature Materials* **8**, 693–695 (2009).

[3] Barraud, C. *et al.* Unravelling the role of the interface for spin injection into organic semiconductors. *Nature Physics* **6**, 615–620 (2010).

[4] Žutić, I., Fabian, J. & Sarma, S. D. Spintronics: Fundamentals and applications. *Reviews of Modern Physics* **76**, 323 (2004).

[5] Awschalom, D. D. & Flatté, M. E. Challenges for semiconductor spintronics. *Nature Physics* **3**, 153–159 (2007).

[6] Nagaosa, N. Spin currents in semiconductors, metals, and insulators. *Journal of Physical Society of Japan* **77**, 031010 (2008).

[7] Maekawa, S., Valenzuela, S., Saitoh, E. & Kimura, T. *Spin Current*, vol. 17 (OUP Oxford, 2012).

[8] Kajiwara, Y. *et al.* Transmission of electrical signals by spin-wave interconversion in a magnetic insulator. *Nature* **464**, 262–266 (2010).

[9] Kurebayashi, H. *et al.* Controlled enhancement of spin-current emission by three-magnon splitting. *Nature Materials* **10**, 660–664 (2011).

[10] Saitoh, E., Ueda, M., Miyajima, H. & Tatara, G. Conversion of spin current into charge current at room temperature: Inverse spin-Hall effect. *Applied Physics Letters* **88**, 182509–182509 (2006).

[11] Kimura, T., Otani, Y., Sato, T., Takahashi, S. & Maekawa, S. Room-temperature reversible spin Hall effect. *Physical Review Letters* **98**, 156601 (2007).

[12] Valenzuela, S. O. & Tinkham, M. Direct electronic measurement of the spin Hall effect. *Nature* **442**, 176–179 (2006).

[13] Ando, K., Watanabe, S., Mooser, S., Saitoh, E. & Sirringhaus, H. Solution-processed organic spin–charge converter. *Nature Materials* **12**, 622–627 (2013).

[14] Sirringhaus, H. *et al.* Two-dimensional charge transport in self-organized, high-mobility conjugated polymers. *Nature* **401**, 685–688 (1999).

[15] Sanvito, S. & Dediu, V. A. Spintronics: News from the organic arena. *Nature Nanotechnology* **7**, 696–697 (2012).

[16] Pramanik, S. *et al.* Observation of extremely long spin relaxation times in an organic nanowire spin valve. *Nature Nanotechnology* **2**, 216–219 (2007).

[17] Nguyen, T. D. *et al.* Isotope effect in spin response of π-conjugated polymer films and devices. *Nature Materials* **9**, 345–352 (2010).

[18] Ando, K. *et al.* Electrically tunable spin injector free from the impedance mismatch problem. *Nature Materials* **10**, 655–569 (2011).

[19] Tserkovnyak, Y., Brataas, A. & Bauer, G. E. W. Enhanced Gilbert damping in thin ferromagnetic films. *Physical Review Letters* **88**, 117601 (2002).

[20] Ando, K. *et al.* Inverse spin-Hall effect induced by spin pumping in metallic system. *Journal of Applied Physics* **109**, 103913 (2011).

[21] Ando, K. & Saitoh, E. Observation of the inverse spin Hall effect in silicon. *Nature Communications* **3**, 629 (2012).

[22] McCulloch, I. *et al.* Liquid-crystalline semiconducting polymers with high charge-carrier mobility. *Nature Materials* **5**, 328–333 (2006).

[23] Harii, K., Ando, K., Inoue, H. Y., Sasage, K. & Saitoh, E. Inverse spin-Hall effect and spin pumping in metallic films (invited). *Journal of Applied Physics* **103**, 07F311 (2008).

[24] Yu, Z. Spin-orbit coupling and its effects in organic solids. *Physical Review B* **85**, 115201 (2012).

[25] P. W. M. Blom, M. J. M. d. J. & van Munster, M. G. Electric-field and temperature dependence of the hole mobility in poly(*p*-phenylene vinylene). *Physical Review B* **55**, R656–R659 (2009).

[26] Wetzelaer, G., Koster, L. & Blom, P. Validity of the einstein relation in disordered organic semiconductors. *Physical Review Letters* **107**, 066605 (2011).

[27] Elliott, R. Theory of the effect of spin-orbit coupling on magnetic resonance in some semiconductors. *Physical Review* **96**, 266 (1954).

[28] Matsui, H. *et al.* Correlation between interdomain carrier hopping and apparent mobility in polycrystalline organic transistors as investigated by electron spin resonance. *Physical Review B* **85**, 035308 (2012).

[29] Brataas, A., Tserkovnyak, Y., Bauer, G. E. W. & Halperin, B. I. Spin battery operated by ferromagnetic resonance. *Physical Review B* **66**, 060404(R) (2002).

[30] Yu, Z. Suppression of the Hanle effect in organic spintronic devices. *Physical Review Letters* **111**, 016601 (2013).

[31] Ando, K. & Saitoh, E. Inverse spin-Hall effect in palladium at room temperature. *Journal of Applied Physics* **108**, 113925 (2010).

[32] Mosendz, O. *et al.* Detection and quantification of inverse spin Hall effect from spin pumping in permalloy/normal metal bilayers. *Physical Review B* **82**, 214403 (2010).

[33] Jiao, H. & Bauer, G. E. Spin backflow and ac voltage generation by spin pumping and the inverse spin Hall effect. *Physical Review Letters* **110**, 217602 (2013).

Acknowledgements

This work was supported by the Cabinet Office, Government of Japan through its "Funding Program for Next Generation World-Leading Researchers", PRESTO-JST "Innovative nano-electronics through interdisciplinary collaboration among material, device and system layers", the Asahi Glass Foundation and the Engineering and Physical Sciences Research Council (EPSRC). The authors thank Dr. Martin Heeney of Imperial College for supplying the PBTTT, Prof. Jairo Sinova of the University of Mainz for stimulating discussions, Dr. Yosuke Kajiwara for helping low temperature measurements, Daichi Hirobe for helping spin pumping measurements, Deepak Venkateshvaran for helping the conductivity measurements, and Olympia Pachoumi for helping with the SEM measurements. K.H.K thanks the Samsung Scholarship Foundation for financial support.

Author contributions

S.W. and K.A. conceived, designed, and performed the experiments, and analyzed the data. S.W., K.A. and H.S. wrote the manuscript. S.W., K.H.K., and S.M. fabricated all devices, performed the electrical characterisation, and wrote supplementary information. Y.V. performed the XPS measurements. H.K. helped low temperature measurements and theoretical part. E.S. and H.S. supervised this work. All authors discussed results and reviewed the manuscript.

Additional information

The authors declare no competing financial interests.

Figure 1: **Spin current transport in trilayer structure.** **a** Schematic illustrations of the $Ni_{80}Fe_{20}$/PBTTT/Pt trilayer device. The PBTTT layer was spin-coated onto a Pt layer. **H** and $\mathbf{M}(t)$ denote the external magnetic field and dynamical magnetization, respectively. $\mathbf{E}_{\rm ISHE}$, $\mathbf{j}_{\rm s}$, and $\boldsymbol{\sigma}$ denote the electric field due to the spin-charge conversion, the flow direction of the spin current, and the spin-polarisation vector of the spin current, respectively. **b** Chemical structure of PBTTT. **c** A cross-sectional transmission electron microscope image of the present $Ni_{80}Fe_{20}$ (10 nm)/PBTTT (20 nm)/Pt (7 nm).

Figure 2: **Observation of spin current transport in PBTTT.** **a** Field (H) dependence of the FMR signal I measured for the $Ni_{80}Fe_{20}$ (10 nm)/PBTTT (40 nm)/Pt (7 nm) trilayer at 100 mW microwave excitation. I is the microwave absorption intensity. The external magnetic field was applied along the film plane, as defined in **b**. The FMR field ($H_{\rm FMR}$ is measured to be 125 mT. **c-f** H dependence of the electromotive force V measured for **c** the $Ni_{80}Fe_{20}$ (10 nm)/PBTTT (40 nm)/Pt (7 nm), **d** $Ni_{80}Fe_{20}$ (10 nm)/PBTTT (40 nm)/Au (40 nm), **e** $Ni_{80}Fe_{20}$ (10 nm)/PBTTT (40 nm)/Cu (300 nm), and **f** $Ni_{80}Fe_{20}$ (10 nm)/CYTOP (60 nm)/Pt (7 nm) trilayers under 100 mW microwave excitation. A chemical structure of CYTOP is shown in the inset of **f**. Here, the black and red circles are the experimental data with the in-plane field **H** and $-\mathbf{H}$, respectively. The direct contribution from ISHE in the Pt layer was extracted by fitting the measured field dependence of the voltage using symmetric and asymmetric Lorentz-type functions. A constant offset voltage due to the microwave irradiation (typically $\sim$ 100 nV) was also subtracted. **g** The equivalent circuit of the present trilayer structure, where $I_{\rm F}$, and $I_{\rm N}$ are the charge currents that are generated due to the spurious effects at the $Ni_{80}Fe_{20}$ layer and due to the ISHE at the Pt layer, respectively. $R_{\rm PBTTT}$, $R_{\rm F}$, and $R_{\rm N}$ are the electrical resistance of the PBTTT, $Ni_{80}Fe_{20}$ and Pt layers. $V_{\rm out}$ is the output voltage in the Pt layer. **h** PBTTT thickness $d_{\rm s}$ dependence of the magnitude of the electric voltage $V_{\rm ISHE}$ normalized by the value of $V_{\rm ISHE}$ at $d_{\rm s}$ = 20 nm. Devices with different film thicknesses were fabricated by varying the spin-coating speed when depositing the PBTTT layer. For all thicknesses the resistances of the Pt layer are essentially the same (40 $\pm$ 3 Ω). The solid circles are the experimental data and the solid curve is an exponential fit.

Figure 3: **Hanle observation in PBTTT. a** The concept of Hanle measurements in the present trilayer. **b** The out-of-plane magnetic field θ dependence of V_{ISHE} extracted by the fitting procedure from the V spectra measured for the $Ni_{80}Fe_{20}$ (10 nm)/PBTTT (60 nm)/Pt (7 nm) trilayer, where $\bar{V}_{\mathrm{ISHE}}$ represents V_{ISHE} normalized by the microwave absorption at each θ. The solid circles are the experimental data. The solid curve is the theoretical curve obtained with the longer spin relaxation time $\tau = 1$ ns (orange) and 1 μs (red). The dotted curves show the theoretical curve with the shorter $\tau = 1$ ps (blue), 0.1 ns (right blue), and 0.5 ns (green). The theoretical calculation was carried out using equation (2) with experimental results $x = d_{\mathrm{s}} = 60$ nm, $\lambda_{\mathrm{s}} = 153$ nm, and $\omega_{\mathrm{L}} = 2.2 \times 10^{10}$ s^{-1}. **c** θ dependence of the ferromagnetic resonance field H_{FMR}. The solid circles are the experimental data and the solid curve is the numerical solution of the Landau-Lifshitz-Gilbert equation. **d** θ dependence of the magnetization angle ϕ. The dashed line shows $\theta = \phi$. The definition of θ and ϕ are also shown in **a**.

Figure 4: **Temperature dependences of spin current transport. a** Temperature T dependence of $\bar{V}_{\mathrm{ISHE}}$ normalized, measured for the $Ni_{80}Fe_{20}$ (10 nm)/PBTTT (d_{s} nm)/Pt (7 nm) trilayers with varying the PBTTT thickness d_{s}. The measurements were performed using a coplanar waveguide with $f = 3$ GHz, and $P = 20$ dBm. **b** d_{s} dependences of V_{ISHE}/P at different temperatures. Solid circles are the experimental data and solid curves are the exponential fitting results. **c** Current-voltage (J-V) characteristics of the $Ni_{80}Fe_{20}$ (10 nm)/PBTTT (120 nm)/Pt (7 nm) trilayer with different temperatures. The inset magnifies the small current region. J-V curves were measured with a cross-bar configuration, where the junction size is 100 μm $\times$ 100 μm. A positive bias corresponds to the positive bias at the Pt electrode. **d** T dependences of the spin diffusion length λ_{s}, mobility μ, and spin lifetime τ_{s} (from the top to bottom). Here, λ_{s} is determined from the exponential decay at given temperatures as shown in **b**. μ is determined from J-V curves as shown in **c**. τ_{s} is calculated from the kinetic equation $\lambda_{\mathrm{s}} = \sqrt{D\tau_{\mathrm{s}}}$, where $D = k_{\mathrm{B}}T\mu/e$ is the diffusion coefficient of PBTTT. The error bars represent the fit uncertainty.

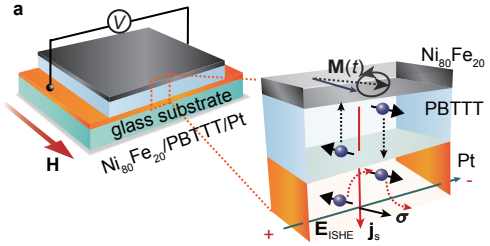
a
V
glass substrate
Ni80Fe20/PBTTT/Pt
H
M(t)
Ni80Fe20
PBTTT
Pt
-
+
E ISHE
j s
σ

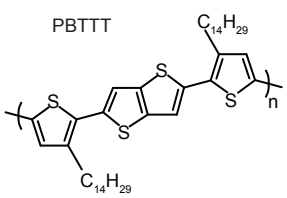
b
PBTTT
C14H29
S
S
S
n
C14H29

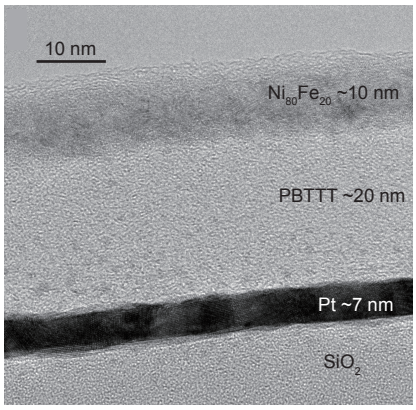
c
10 nm
Ni80Fe20 ~10 nm
PBTTT ~20 nm
Pt ~7 nm
SiO2

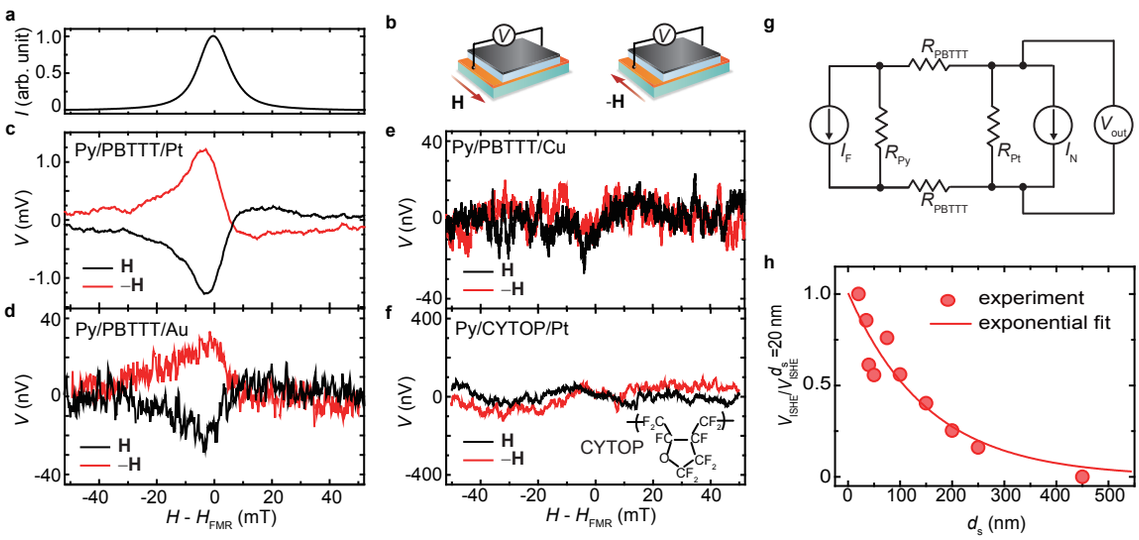
a
I (arb. unit)
1.0
0.5
0
b
V
H
-H
g
R_PBTTT
I_F
R_Py
R_Pt
I_N
V_out
R_PBTTT
c
Py/PBTTT/Pt
V (mV)
1.0
0
-1.0
H
–H
d
Py/PBTTT/Au
V (nV)
40
0
-40
H
–H
-40
-20
0
20
40
H - H_FMR (mT)
e
Py/PBTTT/Cu
V (nV)
40
0
-40
H
–H
f
Py/CYTOP/Pt
V (nV)
400
0
-400
H
–H
CYTOP
F2C
CF2
FC
CF
O
CF2
CF2
-40
-20
0
20
40
H - H_FMR (mT)
h
experiment
exponential fit
V_ISHE/V_ISHE^ds=20 nm
1.0
0.5
0
0
100
200
300
400
500
d_s (nm)

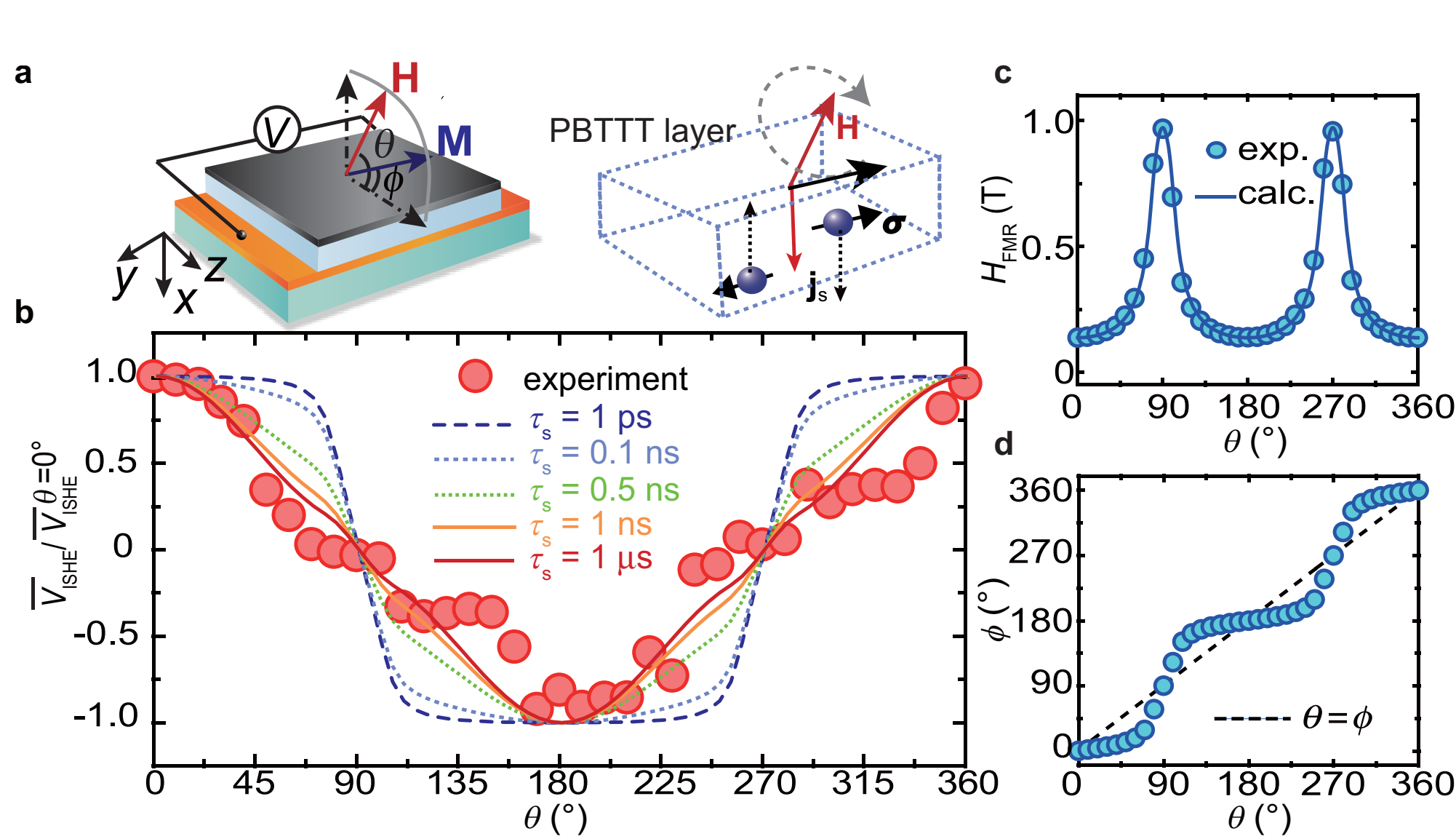
a
H
M
V
θ
ϕ
y
z
x
PBTTT layer
H
σ
j_s
b
experiment
τ_s = 1 ps
τ_s = 0.1 ns
τ_s = 0.5 ns
τ_s = 1 ns
τ_s = 1 μs
$\overline{V}_{ISHE}/\overline{V}_{ISHE}^{\theta=0°}$
θ (°)
c
exp.
calc.
H_{FMR} (T)
θ (°)
d
ϕ (°)
θ=ϕ
θ (°)

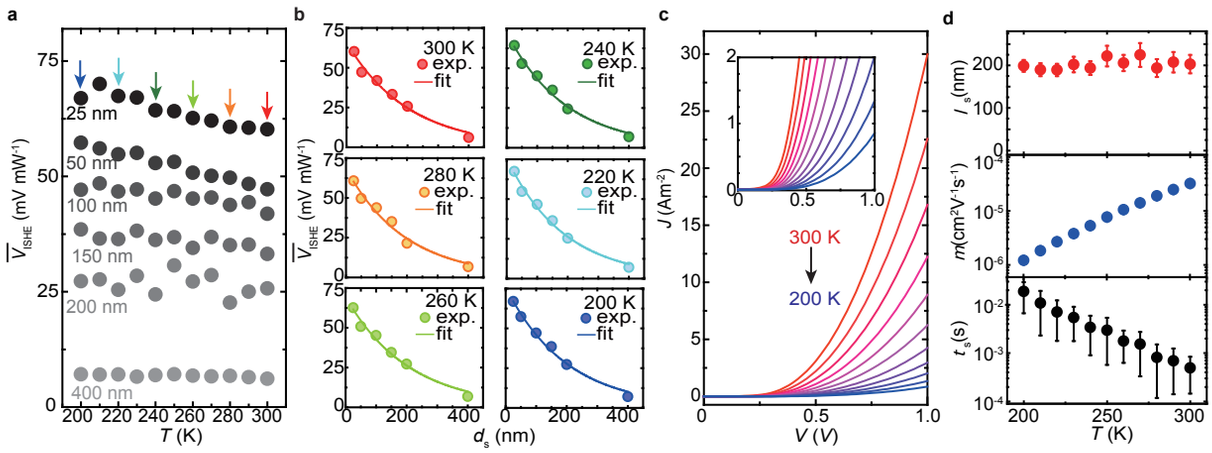
a
b
c
d
25 nm
50 nm
100 nm
150 nm
200 nm
400 nm
T (K)
300 K
240 K
280 K
220 K
260 K
200 K
exp.
fit
d_s (nm)
J (Am^-2)
V (V)
300 K
200 K
l_s (nm)
m (cm^2V^-1s^-1)
t_s (s)